Pedestrian-level wind speed enhancement in urban street canyons with void decks

Citation: Chew, Lup Wai and Leslie K. Norford. "Pedestrian-level wind speed enhancement in urban street canyons with void decks." Building and Environment 146 (December 2018): 64-76

Published Version: http://dx.doi.org/10.1016/j.buildenv.2018.09.039

Publisher: Elsevier BV

Permanent Link: https://hdl.handle.net/1721.1/123467

Version: Author's final manuscript: final author's manuscript post peer review, without publisher's formatting or copy editing

Pedestrian-level Wind Speed Enhancement in Urban Street Canyons with Void Decks

Lup Wai Chew[a,*], Leslie K. Norford[b]

[a] Department of Mechanical Engineering, Massachusetts Institute of Technology, 77 Massachusetts Avenue, Cambridge, MA 02139, USA.

[b] Department of Architecture, Massachusetts Institute of Technology, 77 Massachusetts Avenue, Cambridge, MA 02139, USA.

* Corresponding author. 77 Massachusetts Avenue, 5-418, Cambridge, MA 02139, USA.
E-mail address: lupwai@mit.edu

ABSTRACT

Low wind speeds can inhibit passive ventilation and reduce thermal comfort in tropical cities. We use both experimental and numerical approaches to investigate pedestrian-level wind speed enhancement with void decks (empty spaces at the ground floors) in urban street canyons. Water channel experiments show that void decks allow wind to pass through them, thereby enhancing pedestrian-level wind speeds up to twofold. Computational fluid dynamics models validated with the experiments were used to conduct two parametric studies. The first study varied the void deck height and showed that the wind enhancement effects increase with taller void decks, as expected. The second study varied the canyon aspect ratio and showed that variations in the canyon aspect ratio had less influence on wind enhancement compared to the variations in the void deck height. This is because a void deck induces a secondary vortex, which counter-rotates with the vortex driven by the freestream. Increasing the canyon aspect ratio stretches the vortices vertically but does not alter the (normalized) flow fields. Our findings reveal the potential of void decks to channel wind into street canyons, including narrow (high height-to-width aspect ratio) canyons, which suffer from poor ventilation. The enhanced wind speeds are beneficial for pollutant dispersion and outdoor thermal comfort in tropical cities.

Keywords: Void ground floor, Building porosity, Urban street canyon, Water channel experiment, CFD simulation

Highlights

- Voids at ground floor (void decks) allow winds to flow “through” buildings
- Void decks enhance pedestrian-level wind speeds in urban street canyons
- Void decks are equally effective in narrow urban street canyons
- Wind enhancement effects increase with increasing void deck height

1. Introduction

Wind speeds in urban areas are significantly reduced due to blockage effects of buildings and other urban structures [1–3]. Such blockage effects are apparent in a wide range of scales, from the street level (~100 m) to the regional level (~100 km) [4]. While wind speed reduction may be beneficial in temperate climates (e.g., improved outdoor thermal comfort during winter [5]), it has many negative consequences in tropical climates. For example, urban areas suffer from the urban heat island (UHI) effect, where an urban area is warmer than the surrounding rural area [6,7]. For a given temperature, lower wind speeds further reduce outdoor thermal comfort and decrease the convection heat transfer from building surfaces to the environment, which could increase the cooling demand for buildings. In addition, lower wind speeds inhibit the ability of an urban area to self-ventilate, causing pollutants to be trapped [8,9]. Urban areas thus possess much higher levels of pollutant concentration than rural areas, threatening

the health of city dwellers [10,11]. These factors lead to the guideline "the more wind the better" for tropical cities with weak winds such as Hong Kong [2].

Due to its importance to humans' comfort and safety, wind distribution at the pedestrian level has been studied extensively. The pedestrian level is 1-2 m above ground, where city dwellers perform outdoor activities, from commuting to socializing. The layout of buildings plays an important role in the wind distribution at the pedestrian level. For example, the layout of non-parallel buildings could either decrease or increase the pedestrian-level wind speed, depending on the wind direction [12,13]. A cluster of buildings arranged in a staggered layout induces different blockage effects compared to buildings arranged in an aligned layout [14,15]. Building design features, such as chamfered or rounded corners [16,17], roof shape [18–20], and building porosity [21,22], also influence the wind field in the vicinity of the buildings. This paper focuses on the potential of building porosity for wind enhancement in tropical cities.

Since blockage effects of buildings cause low pedestrian-level wind speed, it is reasonable to reduce the blockage effects by introducing porosity in buildings. Building porosity is not a new concept, as it has been incorporated in many designs aimed at enhancing indoor ventilation. Murakami et al. [21] summarized the advantages of porous buildings, including enhanced passive ventilation and solar shading. Vertical voids, or atria, are commonly adopted in building design, both for ventilation and economic purposes [23–25]. However, adopting building porosity for outdoor applications has received less attention. This is because outdoor wind enhancement is often considered as undesirable in temperate climates, especially during winters. In tropical climates, however, higher wind speeds are preferable because thermal discomfort due to low temperatures rarely occurs [26,27]. With many cities emerging in the tropics, there is a recent emphasis on adopting building porosity to enhance pedestrian-level wind speed.

Tsang et al. [28] reported that podia at the ground level obstruct wind and are not recommended for areas requiring wind enhancement, while Ng [2] suggested creating voids at the ground level to induce wind channeling effect. A parametric study by Yuan and Ng [22] concluded that building porosity at the pedestrian level greatly enhances airflow but building porosity at a higher level does not. Mirzaei and Haghighat [29] suggested combining horizontal and vertical voids with mechanical fans to enhance pedestrian-level wind speed. A series of recent papers [17,30–33] investigated the potential of "lift-up" buildings. Xia et al. [30] conducted wind tunnel experiments with lift-up buildings supported on cores (pillars). They concluded that lifting up the buildings enhances the surrounding pedestrian-level wind by up to 11% for a single building. Using computational fluid dynamics (CFD) models validated with the experiments in [30], Du et al. [31] reported that the lift-up design is effective for different configurations of buildings, especially under oblique wind directions. The wind enhancement could exceed twofold. However, lower wind speeds were observed downstream due to a different wake structure induced by the lift-up buildings. Tse et al. [32] conducted parametric studies of core height and core planar area in a wind tunnel. Both parameters affect the distribution of high wind speed, with the core height having a more significant effect than the planar area. The highest wind speed is achieved with the largest core height and an intermediate core planar area. Zhang et al. [33] extended the study by varying the building height-to-width aspect ratio. Tall and slender (large aspect ratio) lift-up buildings create smaller regions of very high wind speed, while short and wide (small aspect ratio) lift-up buildings create larger regions of high wind speed. Zhang et al. [17] further considered the effects of core height and wind direction. Zooming in to the area underneath the lift-up buildings, they concluded that lift-up design is effective for buildings with height-to-width aspect ratio between 0.5 and 2.0. Corner modification could improve the effectiveness, with the recessed corner performing the best in both normal and oblique wind directions.

The aforementioned studies on lift-up buildings concluded that voids at the ground floors enhance pedestrian-level wind speeds. All these studies have focused on single buildings. Du et al. [31] showed that a lift-up building modifies the downstream wake pattern in an open area (i.e., with no building

downstream). What happens if there are buildings downstream, and how will the modified wake pattern interact with the downstream buildings? Could building porosity enhance wind speeds in urban street canyons? The novelty of our work is found in our answers to these questions. We study a neighborhood-scale series of voids at ground level, or "void decks" in the colloquial term, which have existed in Singapore's public housing since the late 1960s. Fig. 1(a) shows an example of a public flat with a void deck. Void decks serve as public spaces for social activities [34]. Void decks also provide residents spaces for cultural events such as weddings and funeral wakes in land-scarce Singapore [35]. However, new public flats in Singapore have either much smaller or no void decks [36]. Fig. 1(b) shows an example of a new public flat with shops instead of void decks at the ground floor. Social issues aside, "filling" the void decks could reduce pedestrian-level wind speed. We attempt to quantify the wind enhancement of void decks in urban street canyons with different aspect ratios.

(a) (b)

Fig. 1. (a) A void deck of a public flat in Singapore. (b) A new design of a public flat with shops instead of void deck at the ground floor. Photographs by the authors.

We employ both experimental and numerical methods to study flows across idealized urban street canyons with void decks. A reference case of canyons without void decks serves as a control case. Sections 2 and 3 outline the experimental setup and numerical models. Section 4 discusses the experimental results and numerical model validation. Section 5 discusses two parametric studies of void deck height and effective canyon aspect ratio. The conclusions are provided in Section 0.

2. Experimental Setup

A recirculating water channel in the Hydraulic Engineering Laboratory at the Department of Civil and Environmental Engineering, National University of Singapore, was used for all experiments. The water channel is 15 m long, 0.6 m tall and 0.6 m wide, with a maximum flow rate of 50 L s^{-1}. A partition was installed to reduce the effective width from 0.6 m to 0.3 m to double the flow velocity at the test section. The test section measures 3.6 m long, 0.6 m tall and 0.3 m wide. Fig. 2(a) shows the side-view sketch of the recirculating water channel. The valve was used to control the flow rate. Flow straighteners made with a combination of plastic tubes, wire mesh and honeycombs were arranged at the inlet to minimize span-wise and vertical velocities. Two layers of ceramic marbles (1.27 cm diameter, Fig. 2(b)) accelerate the flow development so the flow profile at the test section is fully developed. The floodgate

controls the water depth. A detailed description of the partition and the flow straighteners is available in [37].

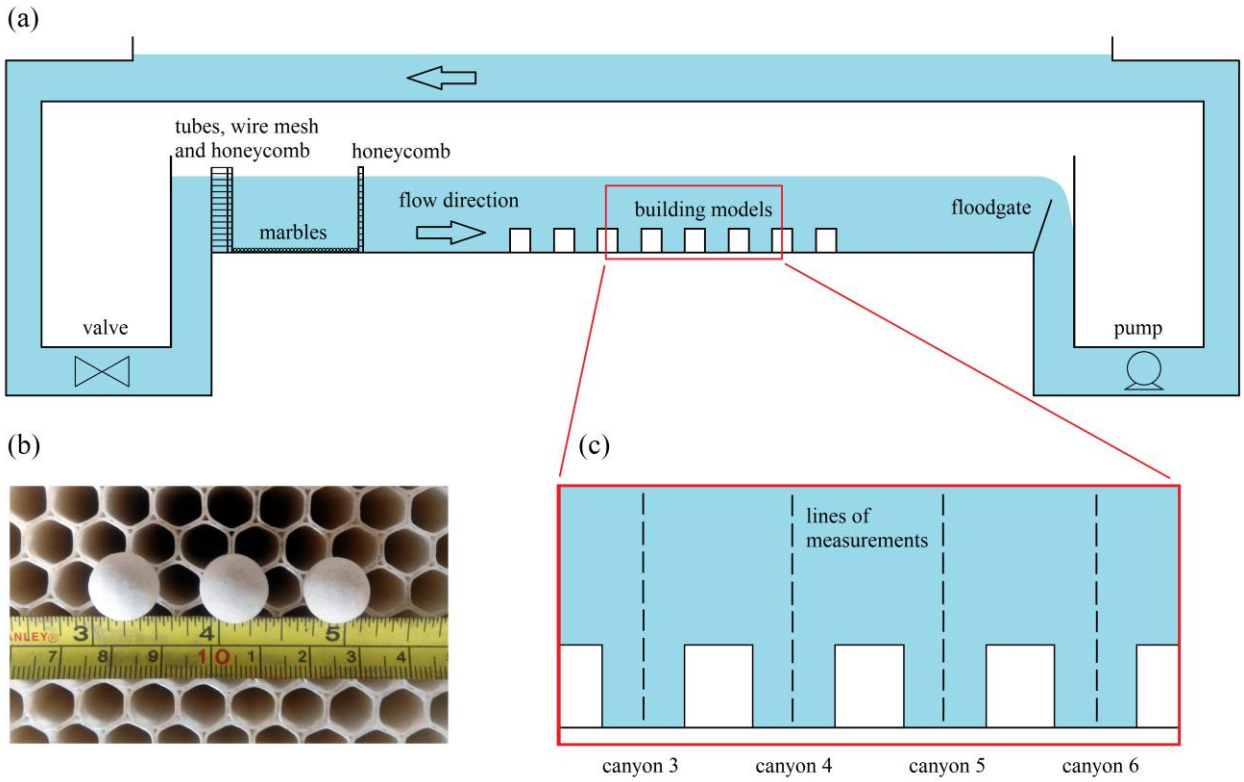

Fig. 2. (a) Side view of the recirculating water channel with an adjustable floodgate and a control valve to vary the flow rate and water depth. The models of buildings were placed in the middle of the test section. (b) Dimensions of the honeycomb and ceramic marbles (top scale in inches, bottom scale in centimeters). (c) Centerlines of canyons 3-6, where the velocity profiles were measured.

The scaled-down model blocks of buildings were made of marine plywood coated with epoxy. The models spanned the whole test section width to simulate two-dimensional (2D) canyons. Two cases were conducted in the water channel: the reference case and the case with void decks. The reference case has seven canyons with height-to-width aspect ratio of 1.0 formed between eight model blocks. All canyons were 12 cm tall, 12 cm wide and 30 cm long. The measurements were taken at the centerlines of canyons 3-6, as shown in Fig. 2(c). The case with void decks has all model blocks lifted up by 2 cm to simulate the void decks, as shown in Fig. 3(a) (only one canyon is shown). The building height, H_b, remained at 12 cm and the void deck height, H_{vd}, was 2 cm. The canyon effective height, $H_{eff} = H_b + H_{vd}$, was 14 cm and the canyon width, W, was maintained at 12 cm. The model blocks were supported on two L-shape aluminum bars fixed to the sidewalls of the test section, as shown in Fig. 3(b). The aluminum bars were 2 mm thick, much smaller than the width of the test section, so they were not disruptive to the flow. Similar to the reference case, the measurements were taken at the centerlines of canyons 3-6. The water depths were 40 cm = $3.3H_{eff}$ and 42 cm = $3.0H_{eff}$ for the reference case and the case with void decks, respectively. The corresponding Froude numbers based on the water depths and freestream velocities were 0.26 and 0.25, which have been verified to be sufficiently small to neglect the free surface effect [38].

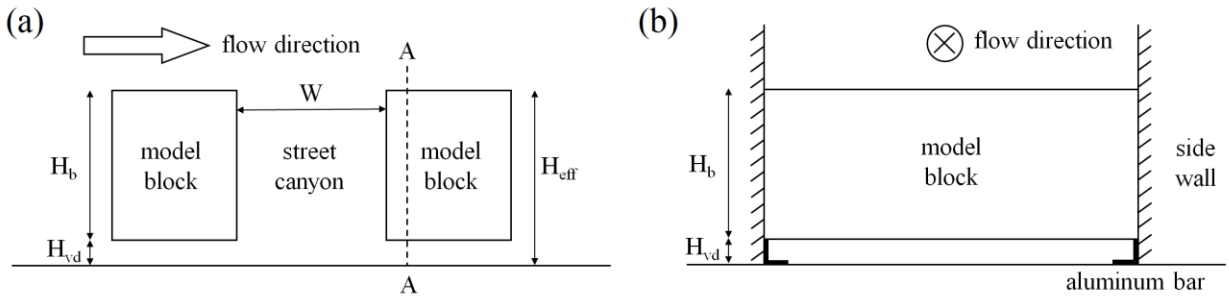

Fig. 3. (a) A street canyon with effective height H_{eff} and width W formed between two building models with building height H_b and void deck height H_{vd}. (b) Cross section across plane A-A viewed in the flow direction (into the page) showing the building model block spans the whole test section width and is bounded by two side walls. The two L-shaped aluminum bars support the lifted model block to simulate void decks.

Acoustic Doppler Velocimeters (ADV, Vectrino by Nortek AS), were used throughout the experiments to measure all three velocity components (stream-wise, vertical, and span-wise). The accuracy is ±0.5% of measured value ±1 mm s^{-1}. The ADV were mounted on metal frames with adjustable vertical position. The measurement frequency was 50 Hz and the measurement period was 60 s, which have been verified to be sufficient to obtain both the mean velocities and turbulence [39]. To check for repeatability of the experimental setup, three sets of measurements were collected for the reference case on three separate days. The three runs produced negligibly small run-to-run standard deviations: 0.001 m s^{-1} for the mean velocities and 0.0005 m s^{-1} for the velocity fluctuations, confirming the repeatability of the experimental setup.

3. Numerical Models

Twelve cases of CFD simulations were conducted, with the parameters H_b, H_{vd}, H_{eff}, W, and H_{eff}/W (see Fig. 3(a) for the nomenclature) listed in Table 1. Case 1 and Case 2 are direct replicates of the reference case and the case with void decks in the water channel experiments. Both have the same dimensions as the corresponding experimental cases and were used for CFD model validations. Due to the limited test section length in the water channel, we could only fit seven canyons in the experiments. The CFD models do not have this constraint, so we repeated Case 2 by increasing the number of canyons to 15 (namely Case 3). This allows us to study a longer array of canyons with void decks. Cases 4-12 are models simulating full-scale canyons. Case 4 is Case 1 scaled up by 200 times (and with eight additional canyons) to simulate full-scale reference canyons. Case 5 is Case 3 scaled up by 200 times to simulate full-scale canyons with void decks. Cases 5-12 are parametric studies of full-scale canyons: Cases 5-9 vary H_{vd} while holding H_b and W constant to study the effects of the void deck height, whereas Case 5 and Cases 10-12 vary H_b while holding H_{vd} and W constant to study the effects of building height and the effective canyon aspect ratio (see Table 1). The reduced-scale Cases 1-3 used the properties of water (to match the experiments), while the full-scale Cases 4-12 used the properties of air.

The CFD models were constructed with ANSYS DesignModeler and meshed with ANSYS Meshing, both in the ANSYS Workbench package 17.2 [40]. The size of the CFD domains followed the recommendations in Franke et al. [41]: the inlet was $5H_{eff}$ upstream of the first building model, the top surface was $6H_{eff}$ from the ground, and the outlet was $15H_{eff}$ downstream from the last building model. The span-wise length was W with a periodic boundary condition in the span-wise surfaces to simulate infinitely long canyons [42–44]. Fig. 4 shows the mesh of the CFD model for Case 2. Inside the canyons and the void decks, the models were meshed with uniform grids of grid size $W/60$. The mesh was coarsened above the canyons, upstream of the first building, and downstream of the last building. The maximum grid expansion ratio was 1.2. The span-wise direction had 25 uniform grids. All grids were perfectly orthogonal with zero skewness. A mesh sensitivity test (provided in the Appendix) was conducted to justify that the mesh resolution is sufficiently high.

Table 1. The building height (H_b), void deck height (H_{vd}), effective canyon height (H_{eff}), canyon width (W), and effective canyon aspect ratio (H_{eff}/W) of the twelve simulated cases.

Case	H_b (m)	H_{vd} (m)	H_{eff} (m)	W (m)	H_{eff}/W	No. of canyons
1	0.12	0	0.12	0.12	1.00	7
2	0.12	0.02	0.14	0.12	1.17	7
3	0.12	0.02	0.14	0.12	1.17	15
4	24	0	24	24	1.00	15
5	24	4	28	24	1.17	15
6	24	2	26	24	1.08	15
7	24	3	27	24	1.13	15
8	24	5	29	24	1.21	15
9	24	6	30	24	1.25	15
10	30	4	34	24	1.42	15
11	36	4	40	24	1.67	15
12	42	4	46	24	1.92	15

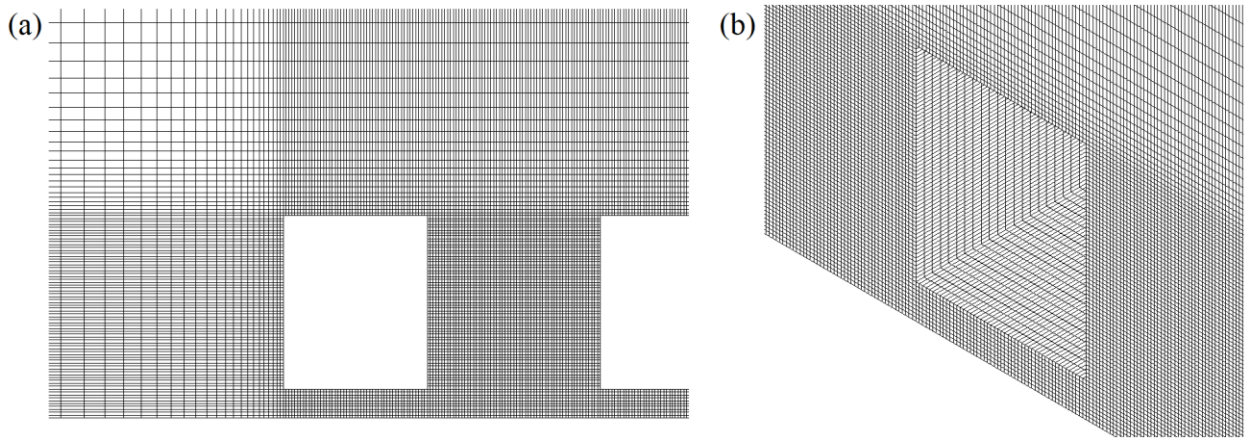

Fig. 4. Mesh of the computational fluid dynamics domain. (a) Side view of the central plane (only the first building and canyon shown) showing uniform mesh in the canyon and coarsened mesh upstream and above the first building. (b) 3D view (only the second canyon shown) showing uniform mesh in the span-wise direction.

The boundary conditions were as follows. The top surface had zero normal velocity and zero gradient for stream-wise velocity (equivalent to the symmetry boundary condition). All walls (leeward walls, windward walls, roofs, grounds) had a no-slip boundary condition. The outlet surface had a zero-gradient boundary condition. For the inlet surface, we used the set of atmospheric inlet boundary conditions [45], where the inlet velocity (U), turbulence kinetic energy (tke), and turbulence dissipation rate (ε) are given in Eqs. (1)-(3) below:

$$U = \frac{U_*}{\kappa} \ln\left(\frac{z + z_0}{z_0}\right) \quad (1)$$

$$tke = \frac{U_*^2}{\sqrt{C_\mu}} \quad (2)$$

$$\varepsilon = \frac{U_*^3}{\kappa(z + z_0)} \tag{3}$$

Here U_* is the friction velocity given in Eq. (4) below, κ the von Karman's constant (= 0.41), z the vertical distance from the ground, z_0 the surface roughness height, and C_μ a constant (= 0.09).

$$U_* = \kappa \frac{U(z = z_{ref})}{\ln\left(\frac{z_{ref} + z_0}{z_0}\right)} \tag{4}$$

Eqs. (1) and (4) can be simplified as a dimensionless velocity profile:

$$\frac{U}{U(z = z_{ref})} = \frac{\ln\left(\frac{z + z_0}{z_0}\right)}{\ln\left(\frac{z_{ref} + z_0}{z_0}\right)} \tag{5}$$

The freestream profile measured at the test section without the building models in the water channel was used to calibrate z_0 and z_{ref}. Eq. (5) best matched the experimental profile with z_0 = 0.0002 m and z_{ref} = 0.14 m. Therefore, Cases 1-3 had z_0 = 0.0002 m and z_{ref} = 0.14 m. $U(z = z_{ref})$ was set at 0.41 m s^{-1} to match the Reynolds number in the water channel experiments. For the full-scale simulations, since the water channel experiments were scaled down by 1:200, Cases 4-12 had z_0 = 0.04 m and z_{ref} = 28 m (both scaled up by 200 times). Note that z_0 = 0.04 m corresponds to open terrain in the updated Davenport-Wieringa classification [46]. $U(z = z_{ref})$ for the full-scale cases was set at 2 m s^{-1}, as field measurements have found that a threshold wind speed of 1.5 to 2 m s^{-1} is needed to sustain the in-canyon vortices [47,48].

The open-source, finite volume solver Open Field Operation and Manipulation (OpenFOAM) version 3.0.1 [49] was used for all CFD simulations. All simulations were run in the Linux platform (Ubuntu 15.10) in a Dell Workstation (Precision Tower 7910) with 48 processors. Forty-four processors were used for each run. The built-in steady Reynolds-averaged Navier-Stokes (RANS) solver, "simpleFOAM," was used with the SIMPLE (Semi-Implicit Method for Pressure Linked Equations) pressure-velocity coupling and k-ε turbulence closure. The three most commonly used k-ε closure schemes are the standard k-ε, Re-Normalization Group (RNG) k-ε, and realizable k-ε. Hang et al. [50] compared the standard k-ε and the RNG k-ε simulations to their wind tunnel experiments and found that the former agreed better with experiments. We tested the standard k-ε and realizable k-ε schemes and found that the former agreed better with our experimental results. Therefore, the standard k-ε was chosen for this study. Second order Gaussian integration with linear interpolation was used for all gradient and divergence schemes. All Laplacian schemes were based on Gaussian integration with linear interpolation and non-orthogonal correction. The standard wall function was employed to reduce computational cost by allowing a coarser mesh. The tolerance of residuals was set at 10^{-5} for all parameters, and iterations were continued until all residuals stopped decreasing with further iterations [51]. The simulation results were post-processed with the open-source software ParaView version 5.3.0 [52].

4. Results and Discussion

4.1 Reference Case

In the water channel experiment, the reference case has seven canyons with aspect ratio of 1.0. The velocity profiles of the centerlines of canyons 3-6 were measured (see Fig. 2(c)). Canyons 1 and 2 were not measured, because they were in the "isolated roughness" regime [53]. We are interested in the "urban roughness" regime [53], which represents wind flows across urban areas. The vertical distance from the ground, z, is normalized by the effective canyon height, H_{eff}. For the experimental results, u is the time-averaged stream-wise velocity, w is the time-averaged vertical velocity and tke =

$0.5(u'^2+v'^2+w'^2)$ is the time-averaged turbulence kinetic energy, where *u'*, *v'*, and *w'* are the root-mean-square stream-wise, span-wise, and vertical velocity fluctuations, respectively. The time-averaged span-wise velocity, *v*, was zero (not shown) due to span-wise symmetry. For the simulation results, *u*, *w*, and *tke* were extracted directly from the steady-state solutions. All profiles were normalized by U_{ref}, which is a reference velocity $2H_{eff}$ above the canyon ground, as recommended in the literature [54,55]. The velocity profiles of canyons 3, 5 and 6 are not shown, since they are similar to the profiles of canyon 4. This similarity is expected, since canyons 3-6 were in the same flow regime.

The results are plotted in Fig. 5. We first compare our experimental results (black circles) to the water channel experiment in Li et al. [54] (blue crosses) in Fig. 5(a) and Fig. 5(b). In our experiments, we used ADV, which is an intrusive measuring device, while they used Laser Doppler Velocimetry (LDV), which is non-intrusive. The profiles of u/U_{ref} and w/U_{ref} from our ADV measurements are consistent with their LDV measurements, confirming that the ADV probes in our experiments did not disrupt the flows.

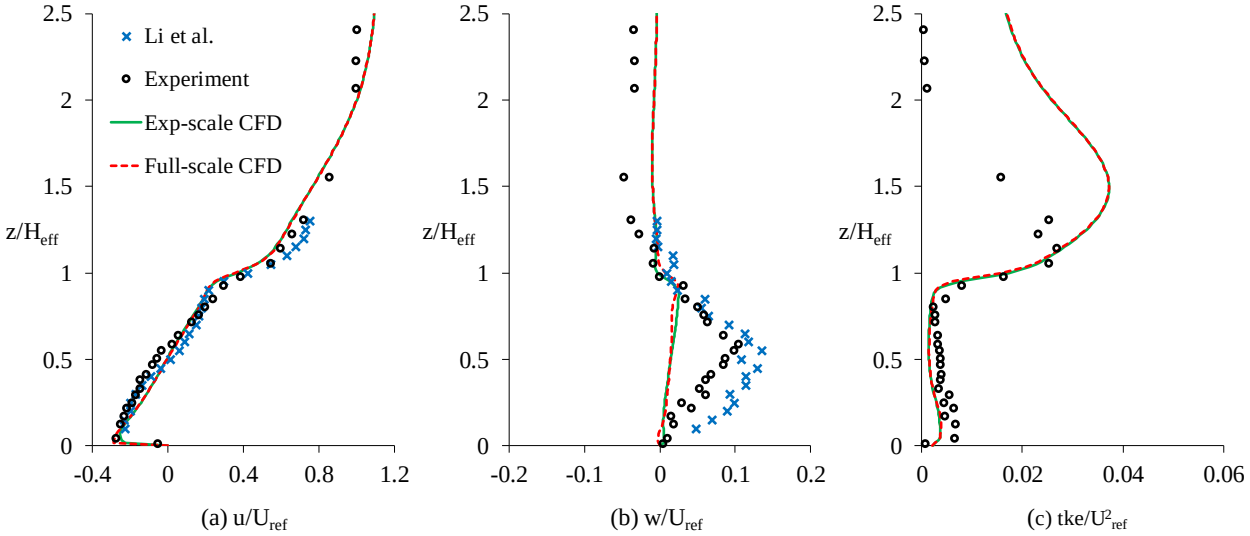

Fig. 5. Normalized middle-line velocity profiles at canyon 4 comparing experimental and CFD results for the reference case. (a) Mean stream-wise velocity, (b) mean vertical velocity, and (c) turbulence kinetic energy. "Li et al." represents water channel experiments from [54], while "Experiment" represents our water channel experimental data. "Exp-scale CFD" and "Full-scale CFD" are CFD simulations at experimental scale and at full scale, corresponding to Case 1 and Case 4 in Table 1.

Next, we validate the CFD simulations at reduced scale (Case 1 in Table 1) and at full scale (Case 4 in Table 1). In Case 1, H_{eff} and the Reynolds number were 12 cm and 62,000. In Case 4, H_{eff} was scaled up by 200 times to 24 m, with a corresponding Reynolds number of 4.3×10^6. Fig. 5(a) shows that the CFD simulations at both scales predict similar u/U_{ref} profiles, which agree well with the experiments. The u/U_{ref} profiles do not change by increasing the Reynolds number from 12,000 (Li et al. [54]) to 62,000 (our water channel experiment) and further to 4.3×10^6 (the full-scale CFD simulation), confirming that the experiments are Reynolds number independent. This is consistent with the Reynolds number independence criterion adopted in the literature, where the flows across canyons with unit aspect ratio are fully turbulent when the Reynolds numbers exceed 10,000 [53,56,57].

Fig. 5(b) shows that the CFD simulations at both scales predicted similar w/U_{ref} profiles. Compared to the experiments, w/U_{ref} was under-predicted by the CFD simulations. Ai and Mak [58] observed zero w/U_{ref} in their RANS simulation, too. They attributed the zero w/U_{ref} to the time-averaged treatment of velocity (steady state) in RANS, which cancels out fluctuating vertical velocity. However, (unsteady) large eddy simulations validated with the same experiment in Li et al. [54] also under-predicted w/U_{ref} [43,59], suggesting that this is not caused by the steady flow assumption in RANS. Li et al. [43] explained that the non-zero w/U_{ref} observed in the experiments was due to a vortex core that has

shifted downstream from the middle canyon axis. Nevertheless, w/U_{ref} is unimportant compared to u/U_{ref} for pedestrian-level winds, so this under-prediction of w/U_{ref} does not affect the conclusion of this study. For the normalized *tke*, Fig. 5(c) shows that the CFD simulations predicted the *tke* inside the canyon well, but over-predicted the *tke* above the roof level. This is due to low freestream *tke* in the water channel experiment, whereas a higher *tke* (calculated by Eq. (2)) was prescribed at the inlet of the CFD models. The *tke* profile given by Eq. (2) is more realistic, as it represents the turbulence in the atmospheric flow.

4.2 Canyons with Void Decks

This section discusses the results for the cases with void decks. In the water channel experiment, all model blocks were lifted up by 2 cm to simulate the void decks with H_{vd} = 2 cm. H_b remained at 12 cm, so H_{eff} was 14 cm. W remained at 12 cm (see Fig. 3). Fig. 6 shows the normalized stream-wise velocity profiles measured at canyons 3-6 in the water channel experiment with Reynolds number 72,000. The corresponding CFD simulation replicating the water channel experiment (Case 2 in Table 1) is overlaid as solid lines. Since our focus is on the pedestrian-level wind speed, the inset in Fig. 6 zooms in to the near-ground level between z/H_{eff} = 0 and z/H_{eff} = 0.25. The inset shows that canyon 3 has the highest near-ground u/U_{ref}, up to 0.5. This means that the near-ground wind speed in canyon 3 is up to 50 percent of the freestream wind speed. Canyon 4 has a lower u/U_{ref}, up to 0.4. The downstream canyons 5 and 6 have lower u/U_{ref} than canyon 4. The trend is clear: the void decks allow wind to flow through them, but the magnitude of wind speed decreases downstream. The CFD simulations show good agreement with the experiment and predict both the enhanced near-ground velocity and the trend of decreasing velocity with downstream canyons.

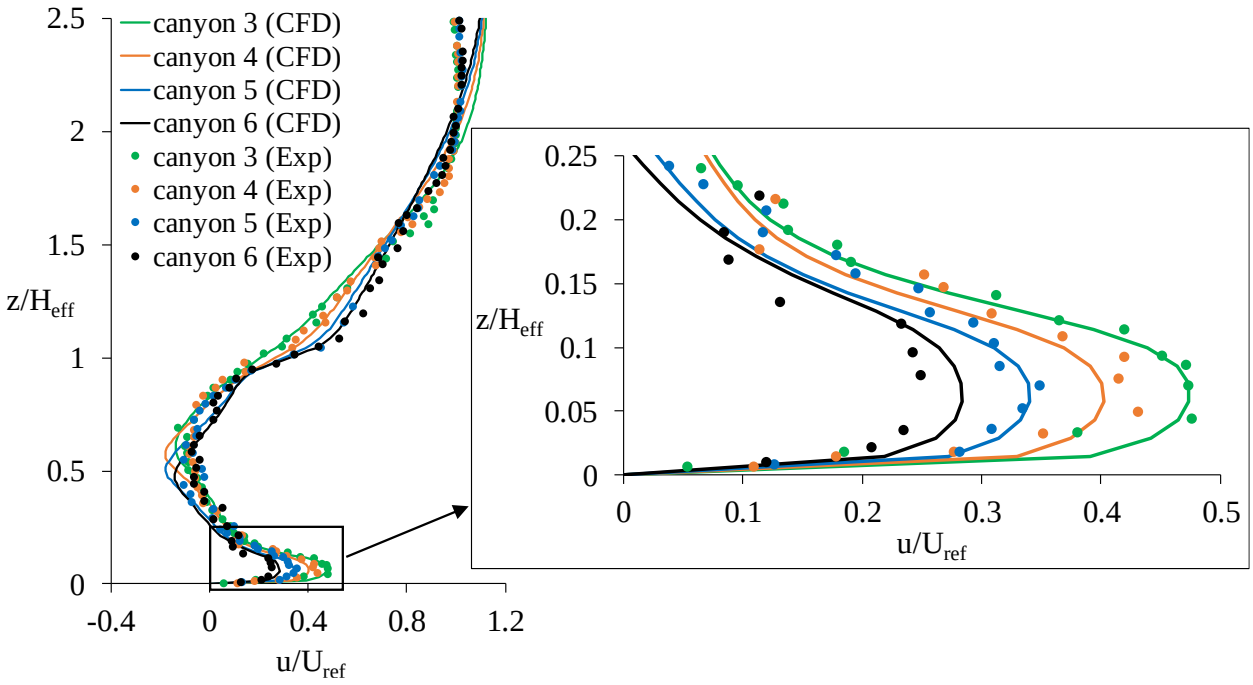

Fig. 6. Normalized mean stream-wise velocity profiles at canyons 3-6 comparing experimental and CFD results for the case with void decks. The inset zooms in to show the trend of near-ground velocity.

The experimental setup with opaque sidewalls did not allow flow visualization. The validated CFD simulations of Case 1 and Case 2 complement the experiments by providing the flow fields. Fig. 7 shows the normalized velocity magnitude contours and vectors at the middle plane of canyons 3-6. Fig. 7(a) shows that in the reference Case 1, all canyons have a similar flow pattern, where a clockwise-rotating vortex is observed in each canyon. Near the ground, the maximum normalized velocity

magnitude, U_{mag}/U_{ref}, is about 0.28. On the other hand, Fig. 7(b) shows that in Case 2 with void decks, the flow fields in canyons 3-6 are different, especially near the ground level. Canyon 3 has the largest near-ground U_{mag}/U_{ref} up to 0.5. Near the windward wall, a portion of the near-ground stream-wise flow leaks and turns into vertical flow, driving a counter-clockwise vortex. This leakage reduces the stream-wise momentum into the downstream void deck. In canyon 4, a similar phenomenon is observed, where a portion of the stream-wise flow turns into vertical flow near the windward wall. Due to the weaker near-ground flow in canyon 4 (compared to that of canyon 3), the counter-clockwise vortex induced by the near-ground flow shrinks, while the clockwise vortex induced by the freestream grows. In canyon 5, the top clockwise vortex has grown larger than the bottom counter-clockwise vortex. The near-ground U_{mag}/U_{ref} in canyon 5 is smaller than that in canyon 4. The reduction of U_{mag}/U_{ref} continues in the downstream canyon 6. In canyon 6, the top clockwise vortex continues to grow while the bottom counter-clockwise vortex almost disappears, and the near-ground U_{mag}/U_{ref} is weaker than that of canyon 5. To summarize, Fig. 7 shows that the void decks allow wind to pass through them, but the wind speed reduces when the wind travels downstream. Two vortices exist in each canyon. The top vortex driven by the freestream grows, while the bottom vortex driven by the near-ground flow shrinks with downstream canyons.

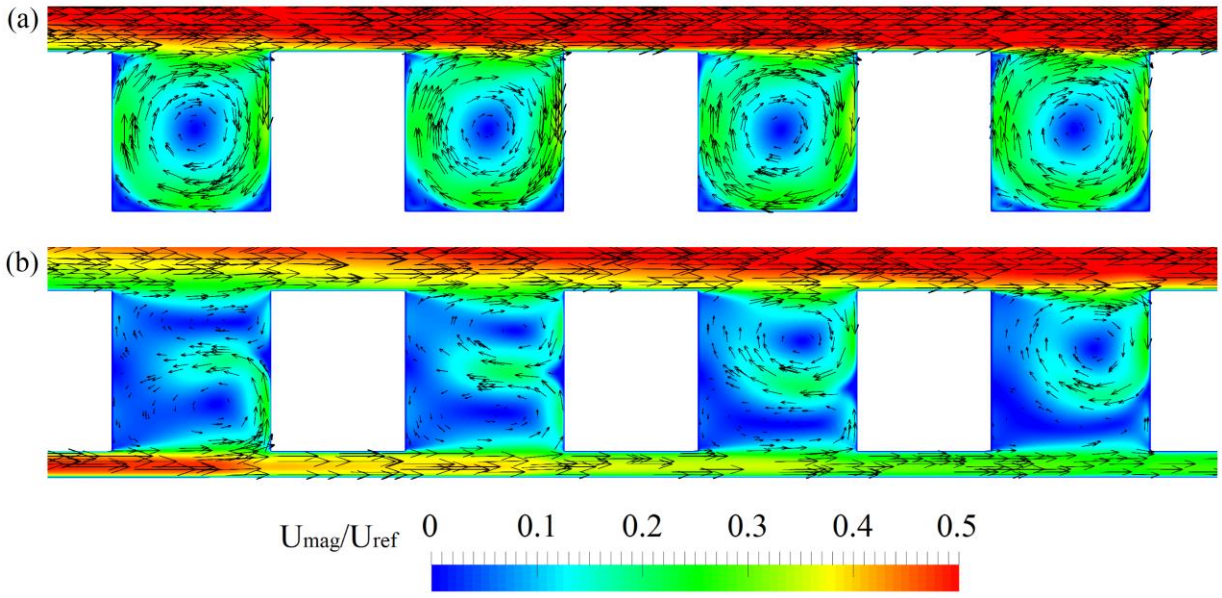

Fig. 7. Normalized velocity magnitude contours and vectors of canyons 3-6 from simulations of (a) reference Case 1 and (b) Case 2 with void decks.

Fig. 7(b) shows that the near-ground velocity reduces while traveling to downstream canyons. Could the near-ground velocity reduce to zero downstream of canyon 6? To answer this question, we extended the CFD domain to consist of 15 canyons (Case 3 in Table 1). In addition, to confirm that the reduced-scale experimental results are applicable at full scale, Case 5 replicated Case 3 with the length scales in all three dimensions scaled up by 200 times, so H_{vd} = 4 m and H_{eff} = 28 m. The Reynolds numbers based on H_{eff} are 72,000 for Case 2 and 5.2×10^6 for Case 5. Fig. 8 plots the profiles at the centerline of canyon 4. Fig. 8(a) shows that at reduced scale, the profiles of Case 2 (green line) and Case 3 (red dashed line) are identical, confirming that extending the simulation domain from seven canyons to 15 canyons did not affect u/U_{ref} profiles. Next, comparing both simulations with 15 canyons in Fig. 8(a), the u/U_{ref} profiles at reduced scale (red dashed lines) and full scale (black dotted lines) are similar. This means that increasing the Reynolds number from 72,000 to 5.2×10^6 does not affect the results. In other words, the reduced-scale experiment and CFD simulations are Reynolds number independent. For w/U_{ref}, Fig. 8(b) shows w/U_{ref} profiles are similar for all three simulated cases. For the normalized *tke*, Fig. 8(c)

shows similar profiles for all three simulated cases, too. To summarize, both extending the CFD simulation domain to include more canyons and scaling up the canyons to full scale do not affect the results. We are now ready to use the validated full-scale CFD models with 15 canyons to perform two parametric studies, which will be discussed in the next section.

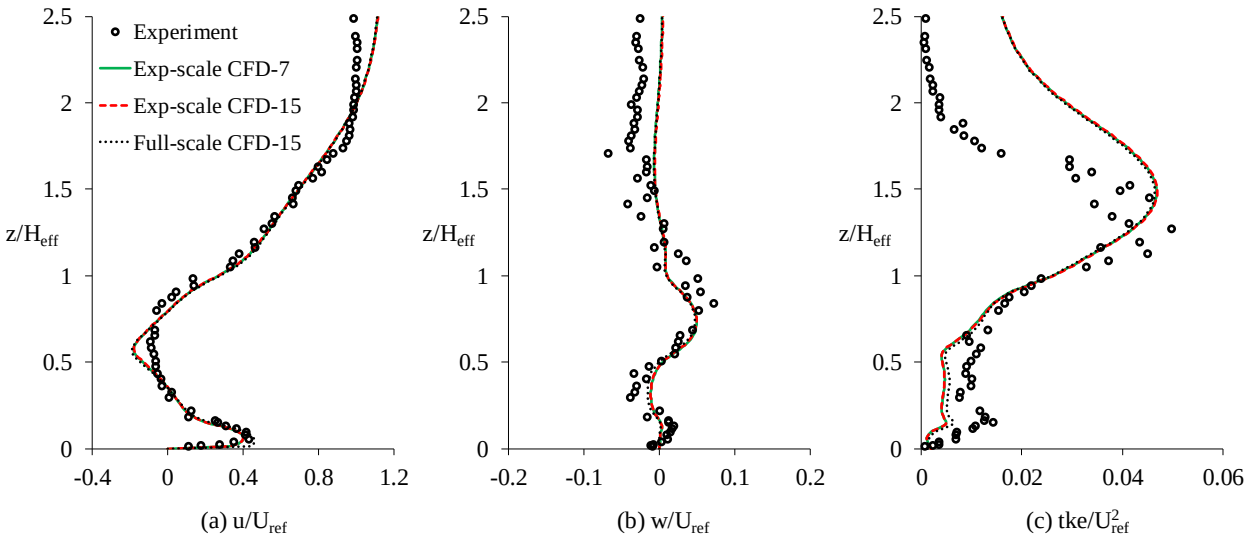

Fig. 8. Normalized middle-line velocity profiles at canyon 4 comparing experimental and CFD results for the cases with void decks. (a) Mean stream-wise velocity, (b) mean vertical velocity, and (c) turbulence kinetic energy. "Experiment" represents our water channel experimental data. "Exp-scale CFD-7" and "Exp-scale CFD-15" represent experimental-scale CFD simulations with seven canyons and 15 canyons (Case 2 and Case 3 in Table 1). "Full-scale CFD-15" represents full-scale CFD simulation with 15 canyons (Case 5 in Table 1).

5. Parametric Study

Two parametric studies at full scale were conducted. The first study with Cases 5-9 varied H_{vd} while holding H_b and W constant to study the effects of void deck height on pedestrian-level wind speed. The second study with Case 5 and Cases 10-12 varied H_b while holding H_{vd} and W constant to study the effects of building height and effective canyon aspect ratio. From Fig. 8, u/U_{ref} is much larger than w/U_{ref}, therefore we compare only u/U_{ref} for these parametric studies. Similar to the reference case, we exclude canyons 1 and 2, since they are in a different flow regime. We also exclude canyon 15, since it is the last canyon in the domain.

5.1 Effects of Void Deck Height

We conducted five full-scale simulations with a fixed H_b = 24 m while varying H_{vd} from 2 m to 6 m with an interval of 1 m. This corresponds to Cases 5-9 in Table 1. Fig. 9 compares u/U_{ref} with different void deck heights at canyons 3 to 14. The u/U_{ref} profiles above the roof level are similar for all five cases and are not shown.

We will first look at Case 6 with 2 m void decks. Fig. 9(a) shows that at canyon 3, the near-ground wind is positive with a maximum u/U_{ref} of 0.33. Fig. 9(b) shows that at canyon 4, the near-ground wind is still positive but with a smaller maximum u/U_{ref} of 0.12. Downstream at canyon 5, Fig. 9(c) shows that the u/U_{ref} profile is different from the profiles in canyons 3 and 4. The sign of near-ground u/U_{ref} in canyon 5 has changed to negative, and the magnitude increases to 0.25. Downstream at canyon 6, Fig. 9(d) shows that the u/U_{ref} profile is similar to the profile at canyon 5. To visualize this transition from positive to negative u/U_{ref} and the change in u/U_{ref} magnitude, we plot the normalized velocity magnitude contours and vectors for canyons 3-6 in Fig. 10(a). Fig. 10(a) shows that the void deck upstream of canyon 3 channels high-speed near-ground flow into canyon 3. This flow pattern in canyon 3 is similar to

that shown in Fig. 7(b). However, at canyon 4, the flow pattern has changed significantly, where the flow exiting the upstream void deck turns into vertical flow. This is due to the opposing flow induced by the clockwise vortex, which is driven by the freestream. Near the ground, the clockwise vortex induces negative stream-wise flow and opposes the positive stream-wise flow exiting from the upstream void deck. The "collision" of two flows with similar strength results in the loss of stream-wise momentum in both flows. At canyons 5 and 6, the flow is analogous to the flow without void decks with a large clockwise vortex (see Fig. 7(a)), indicating that the effect of void decks has become negligible. This flow pattern with negative near-ground u/U_{ref} in canyons 5 and 6 is also observed in downstream canyons 7-14, as plotted in Fig. 9(e)-(l). To summarize the result of Case 6 with 2 m void decks, the near-ground wind speed enhancement is observed only upstream of canyon 4. At canyon 4, the transition to the reference canyon flow (i.e., without void decks) occurs. Downstream of canyon 4, the flow is analogous to the flow in the reference case.

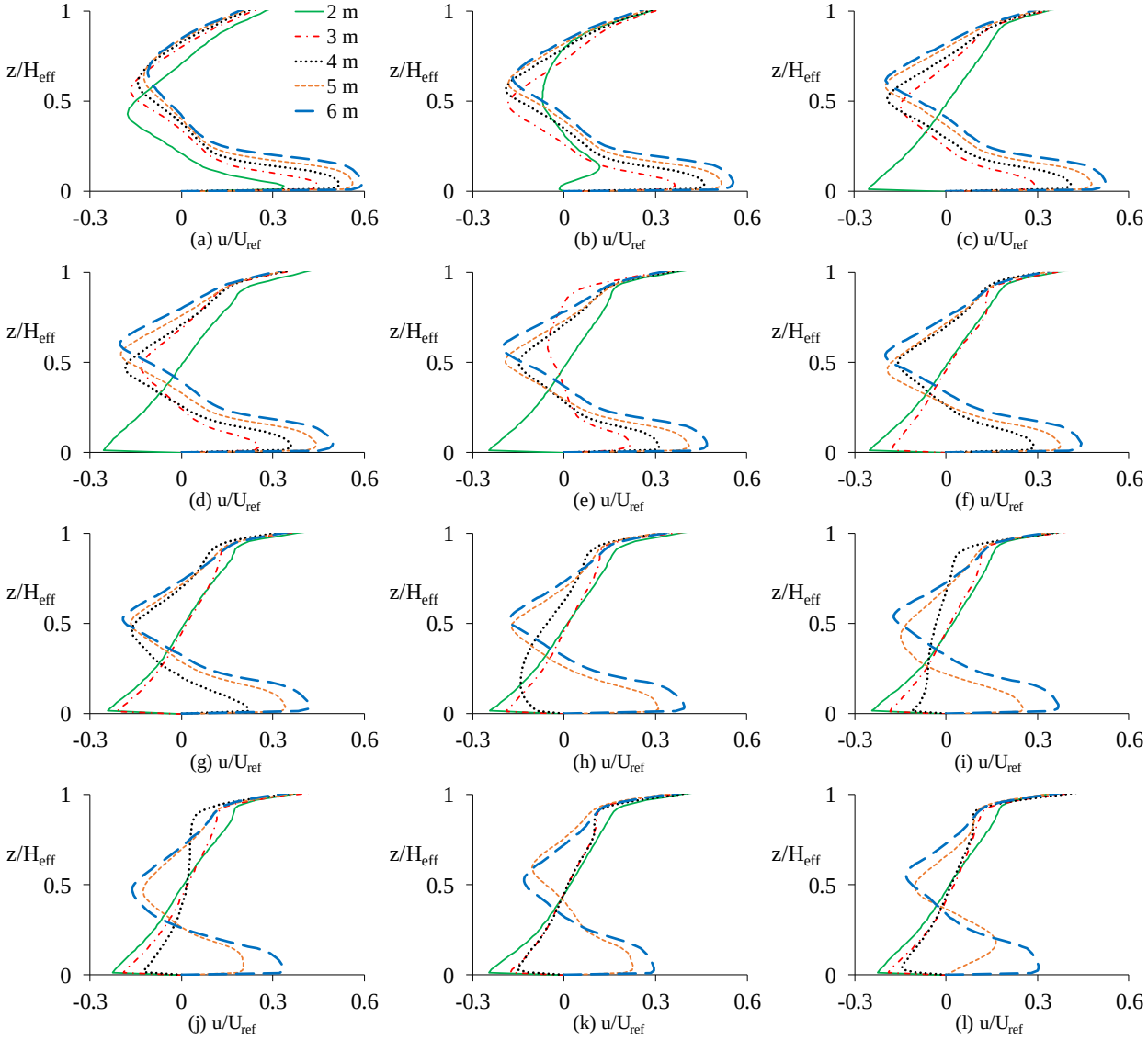

Fig. 9. Normalized mean stream-wise velocity at the centerlines of (a) canyon 3, (b) canyon 4, (c) canyon 5, (d) canyon 6, (e) canyon 7, (f) canyon 8, (g) canyon 9, (h) canyon 10, (i) canyon 11, (j) canyon 12, (k) canyon 13, and (l) canyon 14. The legend indicates the void deck height (H_{vd}). For example, "2 m" represents the case with H_{vd} = 2 m.

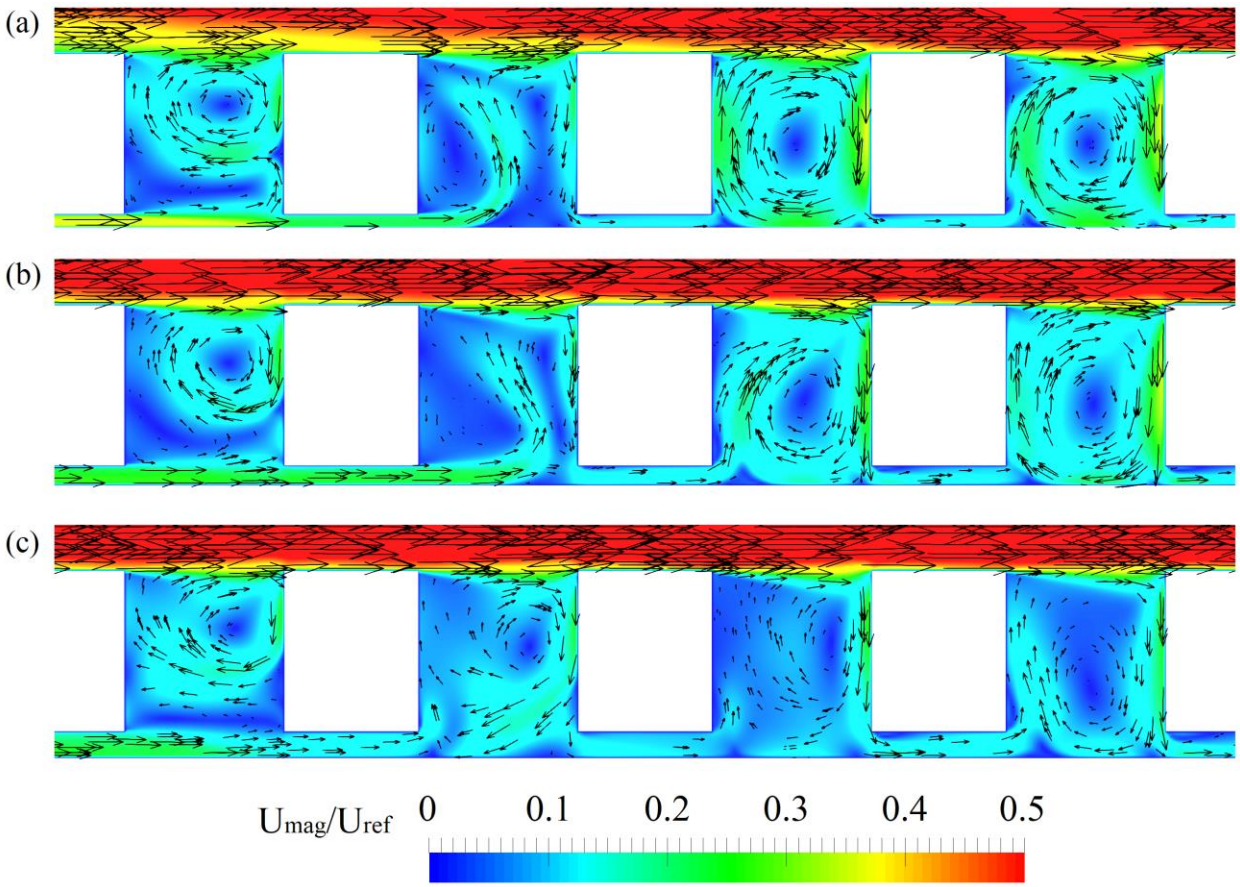

Fig. 10. Normalized velocity magnitude contours and vectors of (a) canyons 3-6 for Case 6 with 2 m void decks, (b) canyons 6-9 for Case 7 with 3 m void decks, and (c) canyons 9-12 for Case 5 with 4 m void decks.

Next, we will look at Case 7 with 3 m void decks. A similar transition to that observed in Case 6 with 2 m void decks is also observed for Case 7. Fig. 9(f) shows that for Case 7, u/U_{ref} changes sign at canyon 8, indicating that the transition occurs at this canyon. The normalized velocity magnitude contours and vectors for canyons 6-9 in Fig. 10(b) confirm that the transition occurs at canyon 8. Similarly, for Case 5 with 4 m void decks, a transition is also observed. Fig. 9(h) shows that for Case 5, u/U_{ref} changes sign at canyon 10, indicating the transition. The corresponding normalized velocity magnitude contours and vectors for canyons 9-12 are shown in Fig. 10(c). For Case 8 with 5 m void decks, no such transition is observed but the profile in Fig. 9(l) suggests that the transition is imminent at canyon 14. For Case 9 with 6 m void decks, no such transition is observed.

We have discussed how the near-ground flows weaken at downstream canyons and eventually trigger the transition to the reference canyon flow. We will now quantify the wind speed enhancement with respect to the reference case without void decks. From Fig. 5(a), the maximum near-ground u/U_{ref} is -0.28 for the reference case without void decks. Since only the wind speed is important but not the wind direction, we can drop the negative sign and take the magnitude of u/U_{ref} = 0.28 for the reference case. From Fig. 9(a), all five cases with void decks show positive near-ground u/U_{ref} at canyon 3. Case 6 with 2 m void decks has the smallest maximum u/U_{ref} of 0.33. This means that at canyon 3, the maximum u/U_{ref} is increased from 0.28 to 0.33 by introducing the 2 m void decks. By defining the enhancement as the wind speed ratio of the case with void decks to that of the reference case, the wind speed ratio is 0.33/0.28 = 1.2. Among the five cases in Fig. 9(a), Case 9 with 6 m void decks has the largest maximum u/U_{ref} of 0.60, or a wind speed ratio of 0.60/0.28 = 2.1. Cases 7, 5, and 8 with 3 m, 4 m, and 5 m void decks have

maximum near-ground u/U_{ref} of 0.45, 0.52, and 0.56, or wind speed ratios of 1.6, 1.8, and 2.0, respectively.

Fig. 11 plots the wind speed ratios for Cases 5-9 at canyons 3-14. As discussed, at canyon 3, the canyons with 2 m, 3 m, 4 m, 5 m, and 6 m void decks have wind speed ratios of 1.2, 1.6, 1.8, 2.0, and 2.1, respectively, which are plotted at the y-axis in Fig. 11. A similar method is used to estimate the wind speed ratios at canyons 4-14. At canyon 4, all canyons observe a drop in wind speed ratios compared to canyon 3. All cases have wind speed ratios larger than 1, except Case 6 with 2 m void decks. A wind speed ratio smaller than 1 means the void decks reduce the near-ground wind speeds relative to the reference case without void decks. At canyon 5, the wind speed ratio in Case 6 recovers to 0.9 after the transition, and stays constant at downstream canyons 6-14. This means that after the transition, the 2 m void decks reduce the near-ground wind speed by about 10 percent relative to the reference canyon.

For Case 7 with 3 m void decks, the transition occurs at canyon 7, as shown in Fig. 10(b). However, the wind speed ratio first drops below 1.0 at canyon 6, indicating that the transition need not happen at the canyon where the wind speed ratio drops below 1.0. Similarly, for Case 5 with 4 m void decks, Fig. 10(c) shows the transition occurs at canyon 10, while Fig. 11 shows the wind speed ratio first drops below 1.0 at canyon 9. For Case 8 with 5 m void decks, the wind speed ratio first drops below 1.0 at canyon 11, but Fig. 9(j) and Fig. 9(k) show no transition at the downstream canyons 12 and 13, while Fig. 9(l) shows that the onset of transition is at canyon 14. No transition is observed for Case 9 with 6 m void decks, and the wind speed ratio is higher than 1 even at the last canyon 14.

Another observation is that after the transition, the wind speed ratio is lower with taller void decks. Comparing the 2 m, 3 m, and 4 m tall void decks, the wind speed ratios after the recovery from the transition are about 0.9, 0.7, and 0.5, respectively. In other words, although taller void decks have higher wind speed ratios prior to the transition, the wind speed ratios after the transition are lower. Since our goal is to enhance near-ground wind speed, we aim to avoid the transition. Provided we know the number of canyons in an array, an optimum H_{vd} can be selected based on Fig. 11. For example, in an array with eight canyons, H_{vd} = 4 m is sufficient to ensure all canyons have wind speed ratio larger than 1.0.

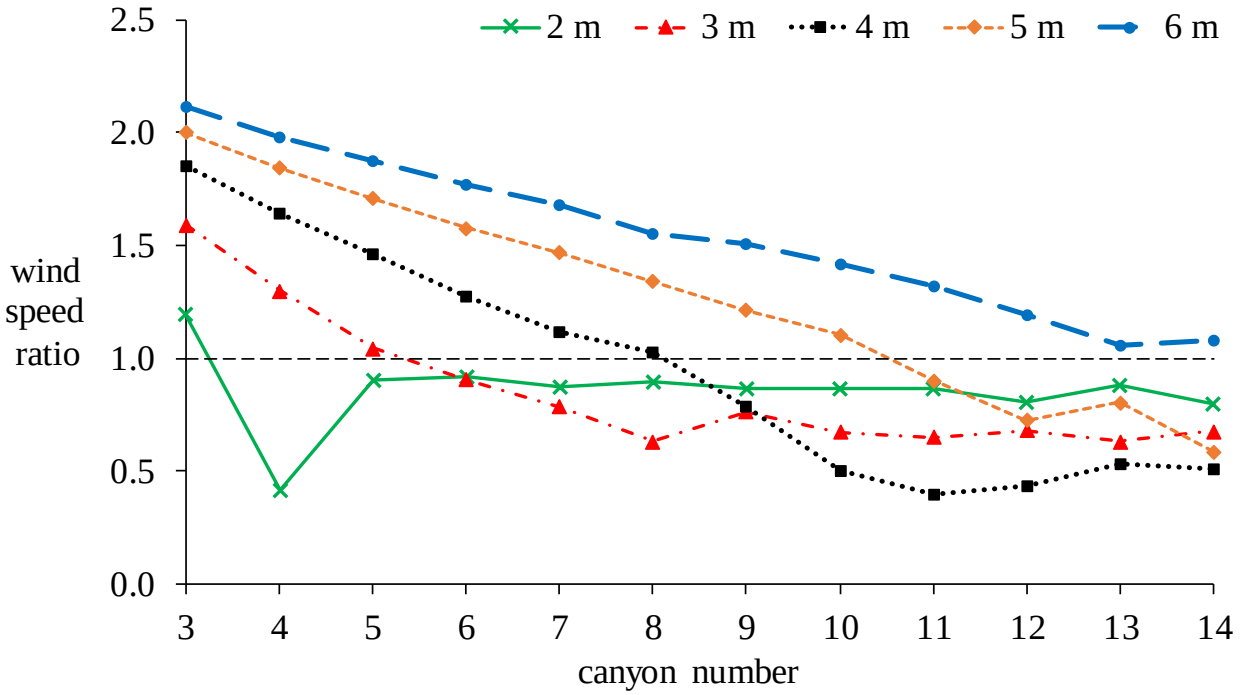

Fig. 11. The wind speed ratio (the ratio of maximum near-ground wind speeds for the cases with void decks to that of the reference case) at canyons 3-14. The legend indicates the void deck height (H_{vd}). For example, "2 m" represents the case with H_{vd} = 2 m.

To summarize, three key observations can be inferred from Fig. 11 for this parametric study. First, prior to the transition, increasing H_{vd} while holding H_b constant increases the wind speed ratio and delays the transition to downstream canyons. Second, prior to the transition, the wind speed ratio decreases almost linearly with downstream canyons. Third, the wind speed ratio is smaller than 1.0 after recovering from the transition, meaning that the near-ground wind speed is higher without the void decks after the transition.

5.2 Effects of building height

For the second parametric study, four values of H_b at 24 m, 30 m, 36 m, and 42 m were simulated, while H_{vd} was fixed at 4 m and W was fixed at 24 m. The effective canyon aspect ratios, H_{eff}/W, ranged between 1.17 and 1.92. These cases correspond to Case 5 and Cases 10-12 in Table 1. Fig. 12 compares u/U_{ref} at canyons 3-14 for the four cases with different H_b. The u/U_{ref} profiles above the roof level are similar for all four cases and are not shown. At canyon 3, Fig. 12(a) shows that all four cases have similar u/U_{ref} profiles and maximum u/U_{ref}. At canyon 4, Fig. 12(b) shows that the maximum u/U_{ref} in all four cases has decreased compared to those in canyon 3, as expected. However, the magnitude of decrease is slightly different: the larger the H_b, the larger the magnitude of decrease. Case 5 with 24 m H_b has the largest maximum u/U_{ref}, while Case 12 with 42 m H_b has the smallest maximum u/U_{ref}. At canyons 5-8, Fig. 12(c)-(f) show the same trend, where the larger the H_b, the smaller the maximum u/U_{ref}. At canyon 9, Fig. 12(g) shows Case 5 with 24 m H_b has a smaller u/U_{ref} than Case 10 with 30 m H_b. This is because the transition occurs at canyon 10 for Case 5, as shown in Fig. 12(h). Fig. 12(i) shows the transition for Case 10 with 30 m H_b occurs at canyon 11, while Fig. 12(j) shows the transitions for Case 11 with 36 m H_b and Case 12 with 42 m H_b occur at canyon 12. After the transition, all four cases have similar profiles, as indicated in Fig. 12(k) and Fig. 12(l).

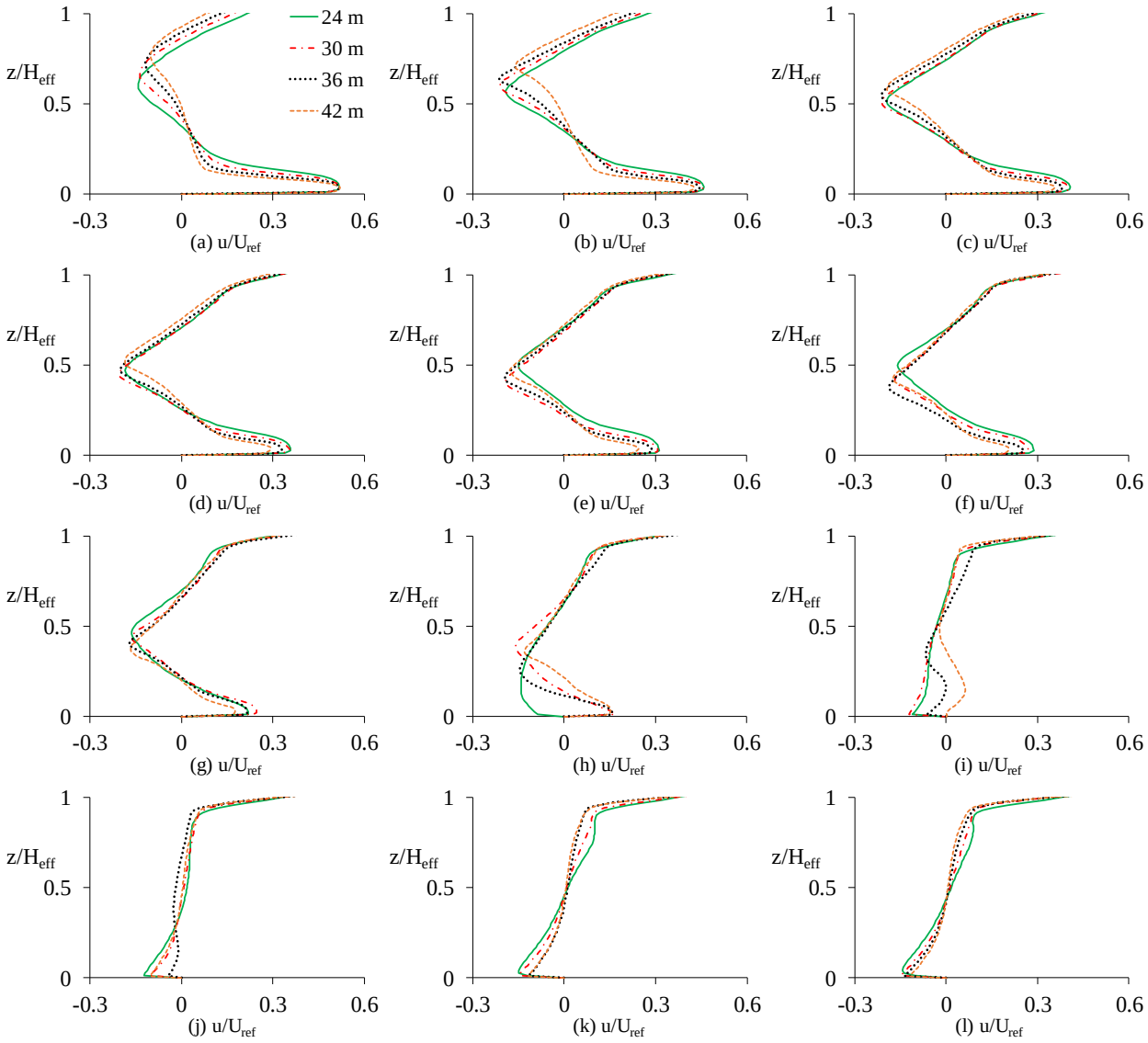

Fig. 12. Normalized mean stream-wise velocity at the centerlines of (a) canyon 3, (b) canyon 4, (c) canyon 5, (d) canyon 6, (e) canyon 7, (f) canyon 8, (g) canyon 9, (h) canyon 10, (i) canyon 11, (j) canyon 12, (k) canyon 13, and (l) canyon 14. The legend indicates the height of building (H_b). For example, "24 m" represents the case with H_b = 24 m.

From Fig. 12(a)-(g), increasing H_b (or equivalently, increasing H_{eff}/W) while maintaining H_{vd} and W does not significantly change the flow pattern and near-ground u/U_{ref} prior to the transition. This is somewhat unexpected, as it is generally understood that the canyon aspect ratio has a strong influence on the in-canyon flow field [38,57,60]. Why does the flow field not depend (or at most, depends weakly) on H_{eff}/W when the canyons have void decks? To answer this question, we shall refer to Fig. 13. Fig. 13 (a)-(d) shows the velocity contours and vectors at canyons 3-6 with H_b of 24 m, 30 m, 36 m, and 42 m. The corresponding H_{eff}/W are 1.17, 1.42, 1.67, and 1.92. Regardless of H_{eff}/W, all four cases observe two counter-rotating vortices in each canyon. The top vortex is driven by the freestream, while the bottom vortex is driven by the near-ground flow from the upstream void deck. Since there are two driving forces (compared to only one in canyons without void decks), there are two in-canyon vortices in all cases. Increasing H_b stretches the vortices in the vertical direction, but after normalizing with H_{eff}, the flow patterns in each canyon are self-similar, which explains the similarity of profiles in Fig. 12(a)-(g). To summarize this parametric study, near-ground u/U_{ref} is insensitive to H_{eff}/W, since there are two counter-

rotating vortices in the canyons. Increasing H_{eff}/W only stretches the vortices vertically with less effects on near-ground u/U_{ref}. This means that void decks are equally effective in channeling atmospheric wind into narrow canyons with large aspect ratio, which inherently suffer from poor self-ventilation.

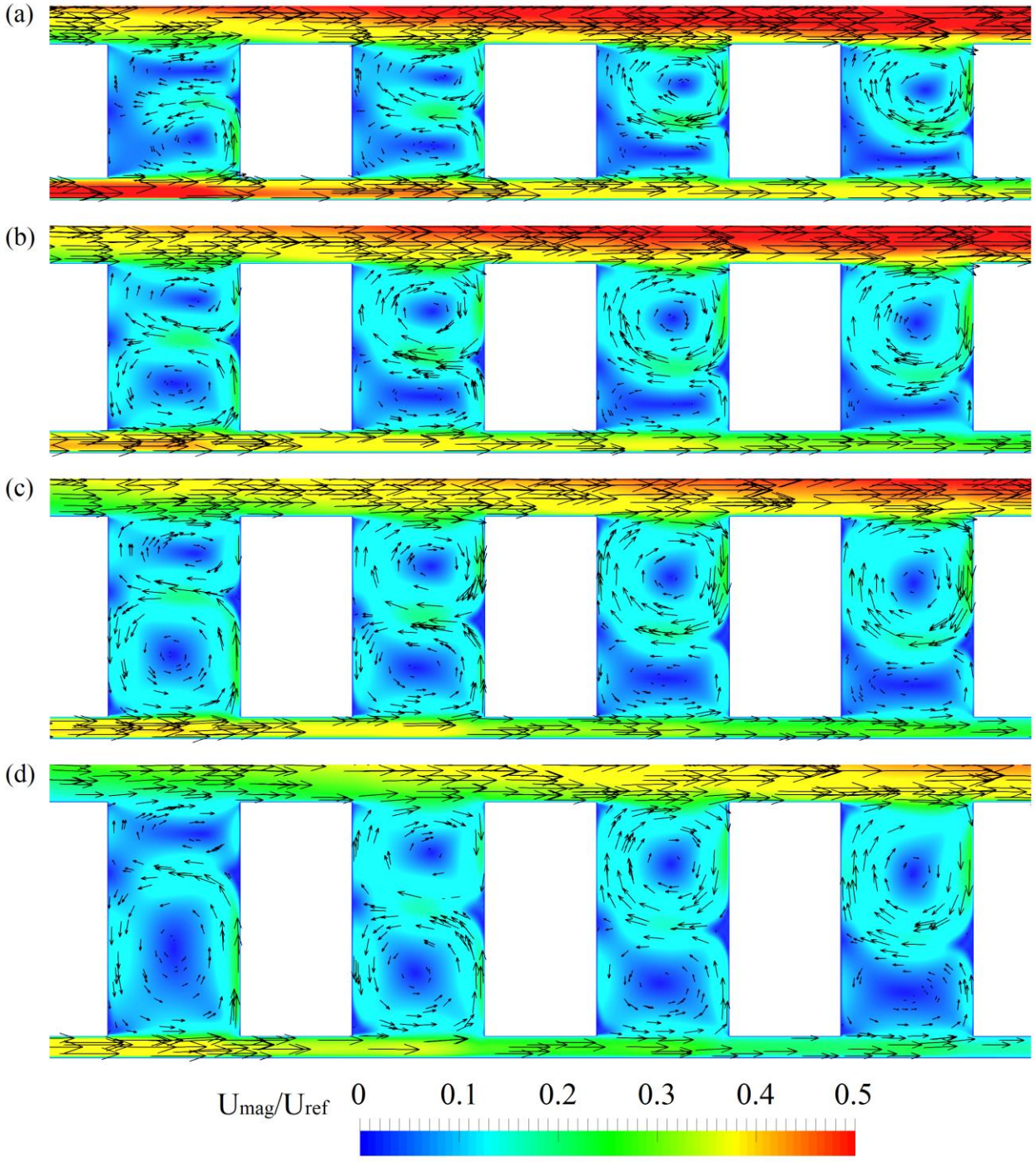

Fig. 13. Normalized velocity magnitude contours and vectors of canyons 3-6 for cases with building heights of (a) 24 m, (b) 30 m, (c) 36 m, and (d) 42 m. All cases have a fixed void deck height of 4 m.

6. Conclusions

Water channel experiments were conducted to study pedestrian-level wind speed enhancement with void decks (voids at the ground floor of buildings, see Fig. 1(a)). In 2D idealized street canyons with unit aspect ratio, the experimental results show that void decks can double pedestrian-level wind speed compared to that in reference canyons without void decks. The experimental results were used to validate computational fluid dynamics models that were then extended to full-scale street canyons in a novel study of the impact of void deck height and building height on airflow in an array of buildings representing residential developments. A summary of key observations is given below:

- The void decks allow wind to flow through them, thereby enhancing near-ground wind speed compared to the reference canyons without void decks. The wind enhancement effects decrease downstream with the weakening of the near-ground wind.
- When the near-ground wind exiting a void deck becomes sufficiently weak, the transition to the reference canyon flow is observed. Downstream of the canyon where the transition occurs, near-ground wind speeds in canyons with void decks are lower than those in the reference canyons.
- Increasing the height of the void decks while keeping the building height constant increases the wind enhancement factors and has a strong effect in delaying the transition.
- Increasing the building height while keeping the height of void decks constant slightly reduces the wind enhancement factors prior to the transition and has a weak effect in delaying the transition.

From the above observations, we have shown that void decks are an effective architectural feature to enhance pedestrian-level wind speeds in urban street canyons. A void deck height of 4 m is sufficient to enhance near-ground wind speeds in an array of fewer than eight canyons. The effective canyon aspect ratio does not affect the flow field prior to transition, meaning that void decks are equally effective in large aspect ratio canyons. Therefore, void decks are useful to channel atmospheric wind into urban street canyons, including narrow canyons with large aspect ratios. Our findings highlight that existing void decks should not be removed, and buildings in tropical cities could incorporate void decks for pedestrian-level wind enhancement in urban street canyons.

Acknowledgment

This research is supported by the National Research Foundation Singapore under its Campus for Research Excellence and Technological Enterprise program. The authors appreciate the discussions with Prof. Rajasekhar Balasubramanian and Dr. Kian Yew Lim, both affiliated with the National University of Singapore (NUS), on the experimental setup and results analyses. Help from the technical staff in the NUS Hydraulic Engineering Laboratory is acknowledged.

Declarations of interest: none

Appendix

Fig. 14 compares the velocity and *tke* profiles of Case 1 from the CFD models with three mesh resolutions. The coarse, normal, and fine mesh models have 0.4 million, 1.6 million, and 5.7 million grids, respectively. Fig. 14(a) shows that u/U_{ref} are identical for the three simulations, except near the ground, where the model with coarse mesh predicted slightly lower u/U_{ref}. Fig. 14(b) shows a larger difference of w/U_{ref} among the models due to very small w/U_{ref}. As discussed in Section 4.1, w/U_{ref} does not affect the conclusions since it is much smaller than u/U_{ref}. Fig. 14(c) shows no significant difference among the normalized *tke* profiles at three mesh resolutions. Overall, the normal mesh resolution used throughout this study is sufficient, as it produced results similar to the fine mesh model.

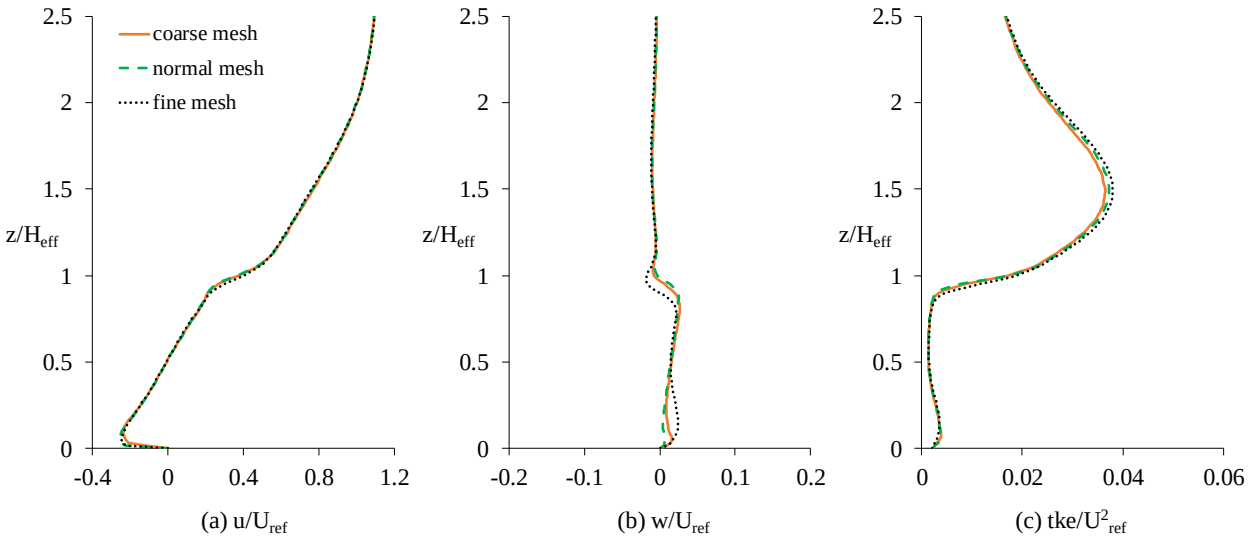

Fig. 14. Normalized middle-line velocity profiles at canyon 4 comparing the CFD results from three mesh resolutions. (a) Mean stream-wise velocity, (b) mean vertical velocity, and (c) turbulence kinetic energy.

References

[1] K.W. Chen, L. Norford, Evaluating Urban Forms for Comparison Studies in the Massing Design Stage, Sustainability. 9 (2017) 987.

[2] E. Ng, Policies and technical guidelines for urban planning of high-density cities–air ventilation assessment (AVA) of Hong Kong, Build. Environ. 44 (2009) 1478–1488.

[3] S.H. Yim, J.C.H. Fung, A.K.-H. Lau, S.C. Kot, Air ventilation impacts of the "wall effect" resulting from the alignment of high-rise buildings, Atmos. Environ. 43 (2009) 4982–4994.

[4] R. Britter, S. Hanna, Flow and dispersion in urban areas, Annu. Rev. Fluid Mech. 35 (2003) 469–496.

[5] T. Stathopoulos, Pedestrian level winds and outdoor human comfort, J. Wind Eng. Ind. Aerodyn. 94 (2006) 769–780.

[6] S. Peng, S. Piao, P. Ciais, P. Friedlingstein, C. Ottle, F.-M. Bréon, H. Nan, L. Zhou, R.B. Myneni, Surface urban heat island across 419 global big cities, Environ. Sci. Technol. 46 (2011) 696–703.

[7] R.A. Memon, D.Y. Leung, C.-H. Liu, Effects of building aspect ratio and wind speed on air temperatures in urban-like street canyons, Build. Environ. 45 (2010) 176–188.

[8] R. Buccolieri, M. Sandberg, S. Di Sabatino, City breathability and its link to pollutant concentration distribution within urban-like geometries, Atmos. Environ. 44 (2010) 1894–1903.

[9] J. Hang, Y. Li, R. Buccolieri, M. Sandberg, S. Di Sabatino, On the contribution of mean flow and turbulence to city breathability: the case of long streets with tall buildings, Sci. Total Environ. 416 (2012) 362–373.

[10] B. Brunekreef, S.T. Holgate, Air pollution and health, The Lancet. 360 (2002) 1233–1242.

[11] P. Carrer, P. Wargocki, A. Fanetti, W. Bischof, E.D.O. Fernandes, T. Hartmann, S. Kephalopoulos, S. Palkonen, O. Seppänen, What does the scientific literature tell us about the ventilation–health relationship in public and residential buildings?, Build. Environ. 94 (2015) 273–286.

[12] B. Blocken, P. Moonen, T. Stathopoulos, J. Carmeliet, Numerical study on the existence of the venturi effect in passages between perpendicular buildings, J. Eng. Mech. 134 (2008) 1021–1028.

[13] B. Li, Z. Luo, M. Sandberg, J. Liu, Revisiting the 'venturi effect'in passage ventilation between two non-parallel buildings, Build. Environ. 94 (2015) 714–722.

[14] M. Lin, J. Hang, Y. Li, Z. Luo, M. Sandberg, Quantitative ventilation assessments of idealized urban canopy layers with various urban layouts and the same building packing density, Build. Environ. 79 (2014) 152–167.

[15] F. Yang, Y. Gao, K. Zhong, Y. Kang, Impacts of cross-ventilation on the air quality in street canyons with different building arrangements, Build. Environ. 104 (2016) 1–12.
[16] T. Tamura, T. Miyagi, The effect of turbulence on aerodynamic forces on a square cylinder with various corner shapes, J. Wind Eng. Ind. Aerodyn. 83 (1999) 135–145.
[17] X. Zhang, K. Tse, A. Weerasuriya, K. Kwok, J. Niu, Z. Lin, C.M. Mak, Pedestrian-level wind conditions in the space underneath lift-up buildings, J. Wind Eng. Ind. Aerodyn. 179 (2018) 58–69.
[18] I. Abohela, N. Hamza, S. Dudek, Effect of roof shape, wind direction, building height and urban configuration on the energy yield and positioning of roof mounted wind turbines, Renew. Energy. 50 (2013) 1106–1118.
[19] A.A. Aliabadi, E.S. Krayenhoff, N. Nazarian, L.W. Chew, P.R. Armstrong, A. Afshari, L.K. Norford, Effects of Roof-Edge Roughness on Air Temperature and Pollutant Concentration in Urban Canyons, Bound.-Layer Meteorol. 164 (2017) 1–31.
[20] Y. Huang, X. Hu, N. Zeng, Impact of wedge-shaped roofs on airflow and pollutant dispersion inside urban street canyons, Build. Environ. 44 (2009) 2335–2347.
[21] S. Murakami, S. Kato, R. Ooka, Y. Shiraishi, Design of a porous-type residential building model with low environmental load in hot and humid Asia, Energy Build. 36 (2004) 1181–1189.
[22] C. Yuan, E. Ng, Building porosity for better urban ventilation in high-density cities–A computational parametric study, Build. Environ. 50 (2012) 176–189.
[23] W. Hung, W. Chow, A review on architectural aspects of atrium buildings, Archit. Sci. Rev. 44 (2001) 285–295.
[24] L. Moosavi, N. Mahyuddin, N. Ab Ghafar, M.A. Ismail, Thermal performance of atria: An overview of natural ventilation effective designs, Renew. Sustain. Energy Rev. 34 (2014) 654–670.
[25] F. Muhsin, W.F.M. Yusoff, M.F. Mohamed, A.R. Sapian, CFD modeling of natural ventilation in a void connected to the living units of multi-storey housing for thermal comfort, Energy Build. 144 (2017) 1–16.
[26] R. de Dear, J. Kim, Thermal Comfort Inside and Outside Buildings, in: Adv. Environ. Wind Eng., Springer, 2016: pp. 89–99.
[27] M. Roth, W.T. Chow, A historical review and assessment of urban heat island research in Singapore, Singap. J. Trop. Geogr. 33 (2012) 381–397.
[28] C. Tsang, K.C. Kwok, P.A. Hitchcock, Wind tunnel study of pedestrian level wind environment around tall buildings: Effects of building dimensions, separation and podium, Build. Environ. 49 (2012) 167–181.
[29] P.A. Mirzaei, F. Haghighat, Approaches to study urban heat island–abilities and limitations, Build. Environ. 45 (2010) 2192–2201.
[30] Q. Xia, X. Liu, J. Niu, K.C. Kwok, Effects of building lift-up design on the wind environment for pedestrians, Indoor Built Environ. 26 (2017) 1214–1231.
[31] Y. Du, C.M. Mak, J. Liu, Q. Xia, J. Niu, K.C. Kwok, Effects of lift-up design on pedestrian level wind comfort in different building configurations under three wind directions, Build. Environ. 117 (2017) 84–99.
[32] K.-T. Tse, X. Zhang, A.U. Weerasuriya, S. Li, K.C. Kwok, C.M. Mak, J. Niu, Adopting 'lift-up'building design to improve the surrounding pedestrian-level wind environment, Build. Environ. 117 (2017) 154–165.
[33] X. Zhang, K. Tse, A. Weerasuriya, S. Li, K. Kwok, C.M. Mak, J. Niu, Z. Lin, Evaluation of pedestrian wind comfort near 'lift-up'buildings with different aspect ratios and central core modifications, Build. Environ. 124 (2017) 245–257.
[34] B. Yuen, Liveability of tall residential buildings, in: High-Rise Living Asian Cities, Springer, 2011: pp. 129–147.
[35] S. Cairns, J.M. Jacobs, J. Yingying, R. Padawangi, S. Siddique, E. Tan, Singapore's Void Decks, in: Public Space Urban Asia, World Scientific, 2014: pp. 80–89.
[36] J. Koh, Void deck, (2015). http://eresources.nlb.gov.sg/infopedia/articles/SIP_2015-01-27_191959.html (accessed October 18, 2016).

[37] L.W. Chew, Passive Enhancement of Air Flow at Pedestrian Level in Built Environments, Master thesis, Massachusetts Institute of Technology, 2017. Available online at https://dspace.mit.edu/handle/1721.1/111767
[38] L.W. Chew, A.A. Aliabadi, L.K. Norford, Flows across high aspect ratio street canyons: Reynolds number independence revisited, Environ. Fluid Mech. (2018). doi:10.1007/s10652-018-9601-0.
[39] L.W. Chew, N. Nazarian, L. Norford, Pedestrian-level urban wind flow enhancement with wind catchers, Atmosphere. 8 (2017) 159.
[40] ANSYS, ANSYS, Inc., 2017. http://www.ansys.com/.
[41] J. Franke, C. Hirsch, A. Jensen, H. Krüs, M. Schatzmann, P. Westbury, S. Miles, J. Wisse, N. Wright, Recommendations on the use of CFD in wind engineering, in: Cost Action C, 2004: p. C1.
[42] J.L. Santiago, A. Martilli, F. Martín, CFD simulation of airflow over a regular array of cubes. Part I: Three-dimensional simulation of the flow and validation with wind-tunnel measurements, Bound.-Layer Meteorol. 122 (2007) 609–634.
[43] X.-X. Li, C.-H. Liu, D.Y. Leung, Large-eddy simulation of flow and pollutant dispersion in high-aspect-ratio urban street canyons with wall model, Bound.-Layer Meteorol. 129 (2008) 249–268.
[44] J. Hang, Y. Li, M. Sandberg, Experimental and numerical studies of flows through and within high-rise building arrays and their link to ventilation strategy, J. Wind Eng. Ind. Aerodyn. 99 (2011) 1036–1055.
[45] P. Richards, R. Hoxey, Appropriate boundary conditions for computational wind engineering models using the k-ϵ turbulence model, J. Wind Eng. Ind. Aerodyn. 46 (1993) 145–153.
[46] J. Wieringa, Updating the Davenport roughness classification, J. Wind Eng. Ind. Aerodyn. 41 (1992) 357–368.
[47] F. DePaul, C. Sheih, Measurements of wind velocities in a street canyon, Atmospheric Environ. 1967. 20 (1986) 455–459.
[48] I. Eliasson, B. Offerle, C. Grimmond, S. Lindqvist, Wind fields and turbulence statistics in an urban street canyon, Atmos. Environ. 40 (2006) 1–16.
[49] OpenFOAM, The OpenFOAM Foundation Ltd, 2017. https://openfoam.org/.
[50] J. Hang, Y. Li, M. Sandberg, R. Buccolieri, S. Di Sabatino, The influence of building height variability on pollutant dispersion and pedestrian ventilation in idealized high-rise urban areas, Build. Environ. 56 (2012) 346–360.
[51] B. Blocken, Computational Fluid Dynamics for urban physics: Importance, scales, possibilities, limitations and ten tips and tricks towards accurate and reliable simulations, Build. Environ. 91 (2015) 219–245.
[52] ParaView, Sandia Corporation, Kitware Inc., 2017. http://www.paraview.org/.
[53] R.N. Meroney, M. Pavageau, S. Rafailidis, M. Schatzmann, Study of line source characteristics for 2-D physical modelling of pollutant dispersion in street canyons, J. Wind Eng. Ind. Aerodyn. 62 (1996) 37–56.
[54] X.-X. Li, D.Y. Leung, C.-H. Liu, K. Lam, Physical modeling of flow field inside urban street canyons, J. Appl. Meteorol. Climatol. 47 (2008) 2058–2067.
[55] P. Kastner-Klein, E. Fedorovich, M. Rotach, A wind tunnel study of organised and turbulent air motions in urban street canyons, J. Wind Eng. Ind. Aerodyn. 89 (2001) 849–861.
[56] W.H. Snyder, Guideline for fluid modeling of atmospheric diffusion, Environmental Protection Agency, Research Triangle Park, NC (USA), 1981.
[57] J.-J. Baik, R.-S. Park, H.-Y. Chun, J.-J. Kim, A laboratory model of urban street-canyon flows, J. Appl. Meteorol. 39 (2000) 1592–1600.
[58] Z. Ai, C. Mak, CFD simulation of flow in a long street canyon under a perpendicular wind direction: Evaluation of three computational settings, Build. Environ. 114 (2017) 293–306.
[59] W. Cheng, C.-H. Liu, Large-eddy simulation of flow and pollutant transports in and above two-dimensional idealized street canyons, Bound.-Layer Meteorol. 139 (2011) 411–437.
[60] X.-X. Li, C.-H. Liu, D.Y. Leung, K. Lam, Recent progress in CFD modelling of wind field and pollutant transport in street canyons, Atmos. Environ. 40 (2006) 5640–5658.